

MnFeNiCuPt and MnFeNiCuCo high-entropy alloys designed based on L₁₀ structure in Pettifor map for binary compounds

A. Takeuchi*, T. Wada, Y. Zhang

Institute for Materials Research, Tohoku University, Sendai, 980-8577, Japan

ARTICLE INFO

Article history:

Received 15 April 2016

Received in revised form

28 September 2016

Accepted 2 December 2016

Available online 8 December 2016

Keywords:

High-entropy alloys

Alloy design

Phase stability

Phase stability, prediction

ABSTRACT

Quinary exact equi-atomic MnFeNiCuPt and MnFeNiCuCo alloys were investigated to examine their formation of high-entropy alloys (HEAs) by focusing on an L₁₀ structure from Pettifor map for binary compounds with 1:1 stoichiometry. The MnFeNiCuPt alloy was practically selected through computer-assisted alloy design under conditions of ≤ 20 at% noble metals, and the condition that the L₁₀ structure appears as frequently as possible in the constituent binary equi-atomic compositions comprised of 78 elements. MnFeNiCuCo was selected by substituting Pt with Co from the MnFeNiCuPt alloy as the second candidate. X-ray diffraction and observations by scanning electron microscopy (by energy dispersive spectroscopy for composition analysis) revealed that as-prepared MnFeNiCuPt and MnFeNiCuCo alloys were formed into HEAs with dual fcc structures containing dendrites of $\sim 10 \mu\text{m}$ in width. The MnFeNiCuPt and MnFeNiCuCo alloys annealed at 1373 K for 43.2 ks and subsequently quenched in water formed single fcc phases and dual fcc phases, respectively. The annealed MnFeNiCuPt and MnFeNiCuCo alloys were subsequently cooled in a furnace and formed single L₁₂ ordered phases and dual fcc phases, respectively. These phases, experimentally observed in the annealed samples, could be partially explained by thermodynamic calculations using Thermo-Calc with SSOL4 and SSOL5 databases for solid solutions. The MnFeNiCuPt and MnFeNiCuCo alloys exhibit soft magnetism with saturation magnetization of 0.23 and 0.43 T, respectively, with coercivity values of $\sim 1 \text{ kA m}^{-1}$. An alloy design for HEAs based on digitalized crystallographic data of these samples could lead to the discovery of new HEAs.

© 2016 Elsevier Ltd. All rights reserved.

1. Introduction

In the last decade, high-entropy alloys (HEAs) [1,2] have been recognized as advanced metallic materials in the field of metallurgy. HEAs are of academic interest due to their combined complexity and conciseness. HEAs are considerably complicated multicomponent alloys due to their number of constituent elements (typically five or more), yet they exhibit simple characteristics for their compositions. They feature exact equi-atomicity and simple crystalline structures such as fcc, bcc and hcp in solid solution forms, rather than the intermetallic compounds that are common to alloys. When designing alloys using a thermodynamic approach, the complexity of HEAs brought about by their multi-component nature makes it difficult to precisely compute the phase stability based on Gibbs free energy. This is because conventional databases [3] in software, such as Thermo-Calc [4], are usually

edited in accordance with each principal element as databases for Fe-base and Ni-base alloys. Recently, a special database for HEAs [3] has been published, and yet the number of elements that can be dealt with is limited to those in existing HEAs only. Thus, it is worth relying on empirical data to develop new HEAs as well as sophisticated computational approaches including Thermo-Calc.

As discussed, three kinds of simple crystalline solid solutions (bcc, fcc, and hcp) are common to HEAs. Some representative HEAs for each structure include AlCoCrFeNi [5] and NbTaTiZrHf [6] alloys for bcc, FeCrMnNiCo [7,8] for fcc, and heavy lanthanide alloys such as YGdTbDyLu, GdTbDyTmLu [9], and HoDyYGdTb [10] for hcp structures. Here, it should be noted that Al_xCoCrCuFeNi alloys [11] are another type of representative HEA, exhibiting bcc, bcc + fcc, and fcc phases as the Al contents decrease, although these alloys do not exhibit exact equi-atomicity depending on this Al content. In different HEAs with exact equi-atomicity, a single fcc phase is relatively difficult to obtain by conventional production methods such as casting, induction melting, or arc-melting, excluding vapor deposition for thin films, mechanical alloying for fragments, and

* Corresponding author. 2-1-1, Katahira, Aoba-ku, Sendai, 980-8577, Japan.

E-mail address: takeuchi@imr.tohoku.ac.jp (A. Takeuchi).

melt-spinning for ribbon samples. Cantor et al. [7] reported that FeCrMnNiCo only exhibits a single fcc solid solution that solidifies dendritically in a melt-spun ribbon sample. Subsequently, Otto et al. [8] produced a single fcc structure in the FeCrMnNiCo HEA as a cylindrical ingot by drop-casting. On the other hand, a CoCuFeNi alloy prepared by induction melting formed fcc structures with similar composition to the alloy and a Cu-rich phase [12], although the number of elements present (four) does not satisfy the rigid definition of HEAs. These early studies motivated the authors to fabricate HEAs with fcc phases by conventional methods such as induction melting, while utilizing an alloy design for HEAs based on Pettifor map [13] based on the authors' previous studies. The present study focuses on an L₁₀ structure as an fcc-derivative alloy system to fabricate HEAs with fcc structures, as the fcc structure is not directly included in the Pettifor map for binary intermetallic compounds with several stoichiometries (1:1 stoichiometry in particular). The authors focused on crystallographic similarities between L₁₀ and fcc structures with similar atomic sites, where the former exhibits an ordered tetragonal structure that is slightly distorted in an axis with lattice constant (*c*) to that of the base (*a*) and the latter is a disordered cubic lattice. The authors expected that alloy searching by focusing on the L₁₀ structure could lead to discovery of HEAs with fcc structures.

The purposes of the present study are to determine HEAs with fcc structures by induction melting, to clarify their thermodynamic properties (among others), and to evaluate alloy designs for HEAs based on Pettifor map for binary compounds with 1:1 stoichiometry.

2. Methods

MnFeNiCuPt and MnFeNiCuCo alloys were investigated in the present study. First, specimens with nominal compositions of Mn₂₀Fe₂₀Ni₂₀Cu₂₀Pt₂₀ and Mn₂₀Fe₂₀Ni₂₀Cu₂₀Co₂₀ (at.%) were prepared by induction melting from raw metals with industrial purity. 10 g samples were formed into button shaped ingots of ~20 mm^φ and ~6 mm height, where their button shape is similar to those prepared by conventional arc-melting with a hemispheroid shape. These prepared alloys are labeled as as-prepared (AP) samples. The ingot was cut into two pieces perpendicular to the base and their structures were examined by X-ray diffraction (XRD) to the cross-sectional area. The morphology of the sample was observed with scanning electron microscope (SEM) and the chemical composition was analyzed by energy dispersive X-ray spectroscopy (EDX) equipped with SEM. Differential thermal analysis (DTA) was conducted at a heating rate (α_h) of 0.333 K/s up to 973 K, followed by $\alpha_h = 0.167$ K/s up to 1773 K and a cooling rate (α_c) of 0.167 K/s down to 973 K. Samples were annealed at a high temperature to confirm the equilibrium phases. The annealing temperature was decided from DTA analysis. During annealing, the as-prepared ingot was mounted in a quartz glass tube capsule, which was then evacuated and sealed. After annealing, the samples were quenched in water and labeled as WQ samples. Specifically, the WQ samples were dipped in water by breaking the capsule immediately to freeze the structure and morphology of the annealed alloys. For comparison, some annealed samples were also cooled in a furnace, and labeled as FC samples.

MnFeNiCuPt and MnFeNiCuCo alloys were selected by the following procedures. MnFeNiCuPt was first selected from the equi-atomic quinary alloys from 77 elements that can be examined with Pettifor map for binary compounds [13] through computational and statistical procedures. Specifically, the authors dealt with all combinations of 5 taken from these 77 elements (77C₅), for an initial population of ~19.76 million. Candidates were then selected from this population by noting the L₁₀ structure (marked with "p3" in

Pettifor map) in the constituent binary equi-atomic alloys (A₅₀B₅₀ at.%) where the L₁₀ structure was selected due to its crystallographic similarity to an fcc structure. In reality, "p3" as a symbol for the L₁₀ structure in Pettifor map was searched for 77C₅ alloys with a self-built program by varying each element in turn. Here, it should be noted that the number of constituent binary pairs in the quinary exact equi-atomic alloy amounts to 10 (5C₂), and that the authors counted the number of appearances of "p3" in the alloys for 77C₅ alloys. In the course of examining the MnFeNiCuCo alloy, the formation of MnFeNiCuCo HEA with a single phase has recently been reported by Tazuddin et al. [14].

At first, the MnFeNiPdPt alloy was selected as the best candidate, since "p3" appeared in the MnFeNiPdPt alloy in its constituent binary systems 7times out of 10. The MnFeNiPdPt alloy had the greatest number of "p3" occurrences in all the 77C₅ alloys. However, the authors intentionally neglected the MnFeNiPdPt alloy, as it contains too much noble metal contents (Pd and Pt) reaching 40 at.%. Five kinds of second-best candidates, CrMnFePdPt, CrMnPdCdPt, CrFePdCdPt, MnFeNiPtAu and MnFePdCdPt, were also neglected for the same reason, although they exhibited 6 out of 10 "p3" appearances. The third-best candidates were 12 kinds of alloys including the MnFeNiCuPt alloy with 5 out of 10 "p3" appearances. Another candidate was determined by replacing Pt in the MnFeNiCuPt alloy with other conventional metallic elements, leading to the selection of a MnFeNiCuCo alloy. The crystallographic features of the constituent binary alloys of the MnFeNiCuPt and MnFeNiCuCo alloys were summarized as follows from Pettifor map. For 1:1 binary compounds, the MnFeNiCuPt possess a L₁₀ (p3) structure for constituent binary systems of MnNi, MnPt, FeNi, FePt and NiPt, whereas the MnFeNiCuCo alloy has MnNi and FeNi for L₁₀ (p3) as well as CsCl (w4) for FeCo. On the other hand, binary compounds with stoichiometries of 3:1 or 1:3 with AuCu₃ (p9) structures may be generated for some of the atomic pairs in the MnFeNiCuPt and MnFeNiCuCo alloys, but the AuCu₃ (p9) structure was neglected in advance due to the expected low possibility of its formation from the equi-atomicity of the MnFeNiCuPt and MnFeNiCuCo alloys. Pettifor maps indicate that the constituent binary alloys of these alloys possess no binary compounds with other stoichiometries (1:2, 3:4, 2:3, 3:5) and their opposite ratios, suggesting a high possibility to form solid solutions.

The preliminary computational analysis for delta parameter (δ) and mixing enthalpy (ΔH_{mix}) from conventional parameters for evaluating HEAs revealed that the values of (δ , ΔH_{mix} /kJmol⁻¹) decreases from (5.4, 2.8) for the MnFeNiCuPt alloy to (4.8, 1.8) for the MnFeNiCuCo alloy. Here, the MnFeNiCuPt alloy with (δ , ΔH_{mix} /kJmol⁻¹) = (4.8, 1.8) is plotted in zone S for disordered HEAs in a δ – ΔH_{mix} diagram [15], suggesting that the MnFeNiCuPt alloy satisfies a necessary condition for HEA formation.

The MnFeNiCuPt and MnFeNiCuCo alloys were thermodynamically analyzed using commercial software (Thermo-Calc 2015b) with a solid solution database (SSOL5). Here, the authors took into account some of the representative compounds, such as Laves phases, in the SSOL5 database as well as simple solid solutions (fcc, bcc, and hcp) for metals and alloys. The MnFeNiCuCo alloy was separately examined with a special database for high-entropy alloys, Ver. 1 (TCHEA1), since all constituent elements (Mn, Fe, Ni, Cu and Co) are present in TCHEA1. The phases in the computation were automatically determined by the software when deciding the constituent elements. In addition, the SSOL4 database was used to derive the interaction parameter (Q) of the atomic pairs in the constituent elements.

The magnetic properties of the MnFeNiCuPt and MnFeNiCuCo alloys were measured using a vibrating sample magnetometer (VSM) at room temperature by applying a maximum field of 12 kOe. The samples were rectangular in shape with dimensions of 10 mm

in height, 3 mm in depth, and 1 mm in width, as cut from the button samples to meet the requirement that the long distance axis of the rectangular samples is parallel to the direction of solidification (bottom to top of the button samples).

3. Results and discussion

The as-prepared MnFeNiCuPt and MnFeNiCuCo alloys were experimentally investigated for their thermal stability and phase transformations with increasing and decreasing temperature. In the DTA analysis, significant changes in DTA signals due to phase transformations were not detected during heating up to 973 K, except for baseline changes as shown in Fig. 1. Around 973 K, artificial decreases in DTA signals are observed during heating due to the changes in α_h from 0.333 to 0.167 K/s. Further increasing the temperature leads to no obvious phase transitions upon heating up to 1500 K for (a) the MnFeNiCuPt and to 1400 K for (b) the MnFeNiCuCo alloy, whereas both alloys exhibited a liquidus temperature on cooling at approximately 1500 K. After DTA analysis, a slight decrease sample weight was detected for both sample types due to the evaporation of Mn. The DTA traces on heating and cooling shown in Fig. 1 indicate that the fcc structures of the MnFeNiCuPt and MnFeNiCuCo alloys at room temperature, as shown in Figs. 2(a) and (d), are stable up to melting, although the alloys contain allotropic elements, such as Mn, Fe and Co. The disappearance of the allotropic transformations when alloyed is presumably due to the high-entropy effects that stabilize the solid solutions in terms of Gibbs free energy as $G = H - TS$ with G (Gibbs free energy), H (enthalpy), T (absolute temperature) and S (configurational entropy) in the MnFeNiCuPt and MnFeNiCuCo alloys. The equilibrium phases of the MnFeNiCuPt and MnFeNiCuCo alloys were examined by annealing the samples at 1373 K for 43.2 ks from DTA analysis.

The crystallographic structures of the phases in the MnFeNiCuPt and MnFeNiCuCo alloys, as-prepared (AP samples), and FC and WQ samples, were analyzed with XRD as shown in Fig. 2. Fig. 2(a,d) reveal that both AP alloys are formed into fcc structures with Miller indices of (1 1 1), (2 0 0), (2 2 0) and (3 1 1) (going from low to high 2θ angles). The lattice constants (a) of the MnFeNiCuPt and

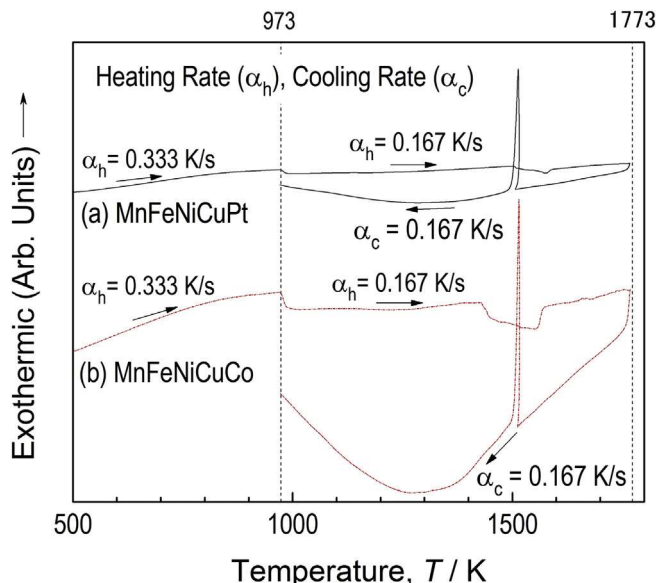


Fig. 1. DTA traces of the MnFeNiCuPt and MnFeNiCuCo alloys on heating and cooling. The heating rate (α_h) of the alloys was 0.167 K/s up to 973 K, followed by $\alpha_h = 0.333$ K/s at 973–1773 K. The cooling rate (α_c) was 0.167 K/s. The artificial decreases in DTA trace at $T \approx 973$ K were due to change in α_h on heating marked by vertical broken lines.

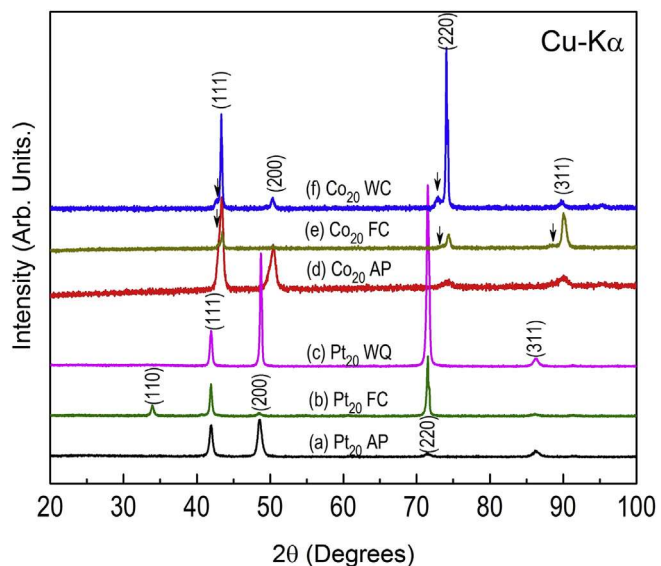


Fig. 2. XRD profiles of the MnFeNiCuPt (Pt₂₀) and MnFeNiCuCo (Co₂₀) alloys (a,d) As-prepared samples (AP). Samples annealed at 1373 K for 43.2 ks and (b,e) subsequently furnace cooled (FC). (c,f) The annealed samples followed by quenching (WQ).

MnFeNiCuCo alloys were evaluated as $a = 0.3739$ and 0.3615 nm, respectively, from 2θ values of the peaks corresponding to the above indices. Fig. 2(a) shows that the XRD peak intensity of the as-prepared MnFeNiCuPt alloy at 2θ is approximately 48.6° for the (2 0 0) reflection, greater than that of $2\theta \approx 41.2^\circ$ for (1 1 1), suggesting the crystallographic orientation of the samples towards [1 1 1]. The formation of the fcc phase in the as-prepared MnFeNiCuPt and MnFeNiCuCo alloys differs from conventional HEAs containing Cr such as AlCoCrFeNi [5] with a bcc structure. In contrast, the as-prepared MnFeNiCuPt and MnFeNiCuCo alloys are akin to the FeCrMnNiCo alloy [7,8] with a fcc structure, and partially agree with the Al_xCoCrCuFeNi alloys [11] with bcc, bcc + fcc and fcc structures with Al contents lower than unity ($x < 1$). This can be explained by the fact that the MnFeNiCuPt and MnFeNiCuCo alloys do not contain Cr as well as Al which are bcc-stabilizing elements, thus enhancing the formations of fcc structures. As such, the MnFeNiCuPt and MnFeNiCuCo alloys differ from most conventional HEAs with fcc structures currently known, such as FeCrMnNiCo [7,8] and Al_xCoCrCuFeNi alloys [11]. Fig. 2(b and c) indicate that the annealed MnFeNiCuPt alloys subjected to FC and WQ exhibit a single phase. Of note, the annealed MnFeNiCuPt alloy subjected to FC has a (110) reflection, which originates from the L₁₂ ordered phase (prototype: Cu₃Au, cP4, Space Group Number: 221). The appearance of L₁₂ order in the MnFeNiCuPt alloy would be affected by the present alloy design, focusing on the L₁₀-ordered phase when selecting the constituent elements. On the other hand, Fig. 2(e and f) indicate that the annealed MnFeNiCuCo alloys subjected to FC and WQ exhibit dual fcc phases. The shoulder peaks in the XRD profiles in Fig. 2(e and f) (denoted with arrows) indicate the presence of dual fcc phases. Fig. 2(a–d) show that MnFeNiCuPt and MnFeNiCuCo alloys are formed in single phases based on XRD analysis.

Further phase analysis was carried out by SEM and EDX; data for the as-prepared samples shown in Fig. 3. These SEM images show few apparent phase separations, except for the artificial contaminations on the surface of the MnFeNiCuCo alloy sample. However, element mappings of the MnFeNiCuPt and MnFeNiCuCo alloys demonstrate the presence of compositional fluctuations in both alloys, where the tendency of the phase separation seems stronger in the MnFeNiCuCo alloy. The as-prepared MnFeNiCuPt and MnFeNiCuCo alloys are composed of dual phases, where Ni is

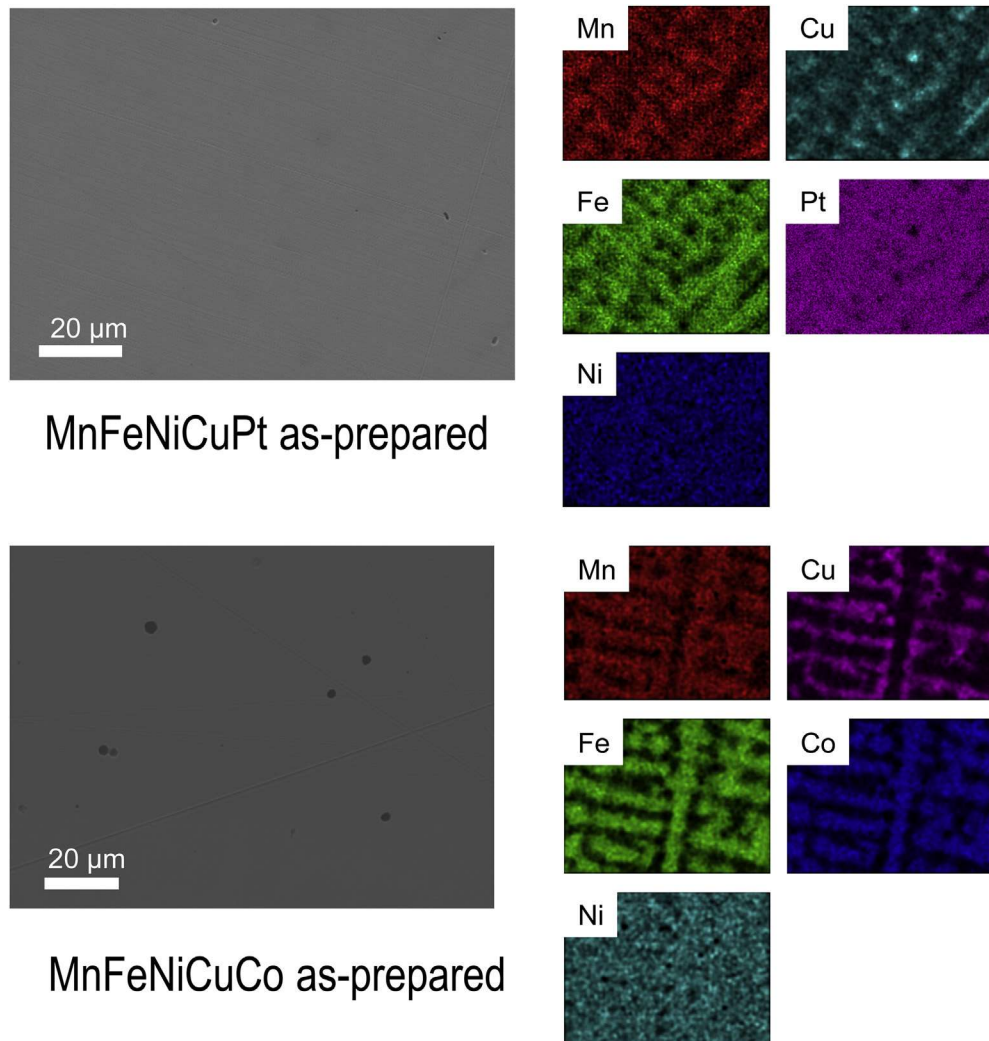


Fig. 3. SEM images and EDX maps of the AP MnFeNiCuPt and MnFeNiCuCo alloys.

homogeneously distributed over the phases. The dual phases of the as-prepared MnFeNiCuCo HEA do not agree with the single-phase HEA reported by Tazuddin et al. [14], although information on its morphology with optical and electron micrographs has not been provided in the literature [14] and the corresponding references in the literature are not accessible. The formation of dual phases in HEAs has frequently been reported as phase separation or elemental segregations, in alloys with immiscible atomic pairs with Cu, such as Fe-Cu and Cu-Co. Examples can be seen in AlCrFeCoNi [16] for bcc and B2 ordered phases, CoCrCuFeNiAl_{0.5} in the nanometer scale [17] for fcc and L1₂ ordered phases, FeNiCoCrCu [18] for Cu-rich and Cu-poor fcc structures, CoCuFeNi with major and minor fcc structures [12] and a series of as-cast alloys with fcc structure comprised of noble metals [19]. Specifically, recent literature [19] has reported that a PdPtRhIrCuNi alloy exhibits a completely dendritic microstructure where the elemental distribution is non-uniform with a dendritic region rich in Rh and Ir but poor in Pd and Cu. However, XRD data of the PdPtRhIrCuNi alloy exhibits a single phase due to non-equilibrium solidification. The experimental data observed in the as-prepared MnFeNiCuPt and MnFeNiCuCo alloys shown in Figs. 2 and 3 tended to show similar XRD and EDX behavior as the PdPtRhIrCuNi alloy [19], suggesting that the single fcc phase from XRD and dual fcc phases from EDX in the as-prepared MnFeNiCuPt and MnFeNiCuCo alloys can arise from

non-equilibrium solidification.

The annealed MnFeNiCuPt and MnFeNiCuCo alloys subjected to WQ were analyzed for their morphology and elemental distributions using SEM and EDX, respectively. Fig. 4 demonstrates that the MnFeNiCuPt alloy was formed into a single phase, whereas the MnFeNiCuCo alloy exhibits phase separation between (Fe,Co,Ni) and (Cu,Mn). The phase separation of the MnFeNiCuCo alloy resulted from the immiscible nature (with large and positive values of ΔH_{mix}) of Fe and Cu along with those of Co and Cu, as shown in Table 1. The elemental maps shown in Fig. 4 indicate that (Cu,Mn) precipitated at the grain boundaries. While not shown in images in Fig. 4, the WQ samples contain some amount of cavities, presumably generated by annealing at higher temperatures (1373 K, close to the solidus temperature). These results reveal that the dual phases of the as-prepared MnFeNiCuPt and MnFeNiCuCo alloys (as shown in Fig. 3) are not stable phases, but are metastable phases or phases generated in a non-equilibrium process during cooling from the melt. The SEM observations and elemental mappings for the annealed MnFeNiCuPt and MnFeNiCuCo alloys subjected to FC in Fig. 5 exhibit similar behavior to the WQ samples.

Details of the analyses in Figs. 2–5 are summarized as follows in terms of their tendencies of phase separation. In Fig. 3, the MnFeNiCuPt alloy demonstrates a weak immiscible tendency between (Fe,Pt) and (Cu,Mn), whereas the MnFeNiCuCo alloy exhibits an

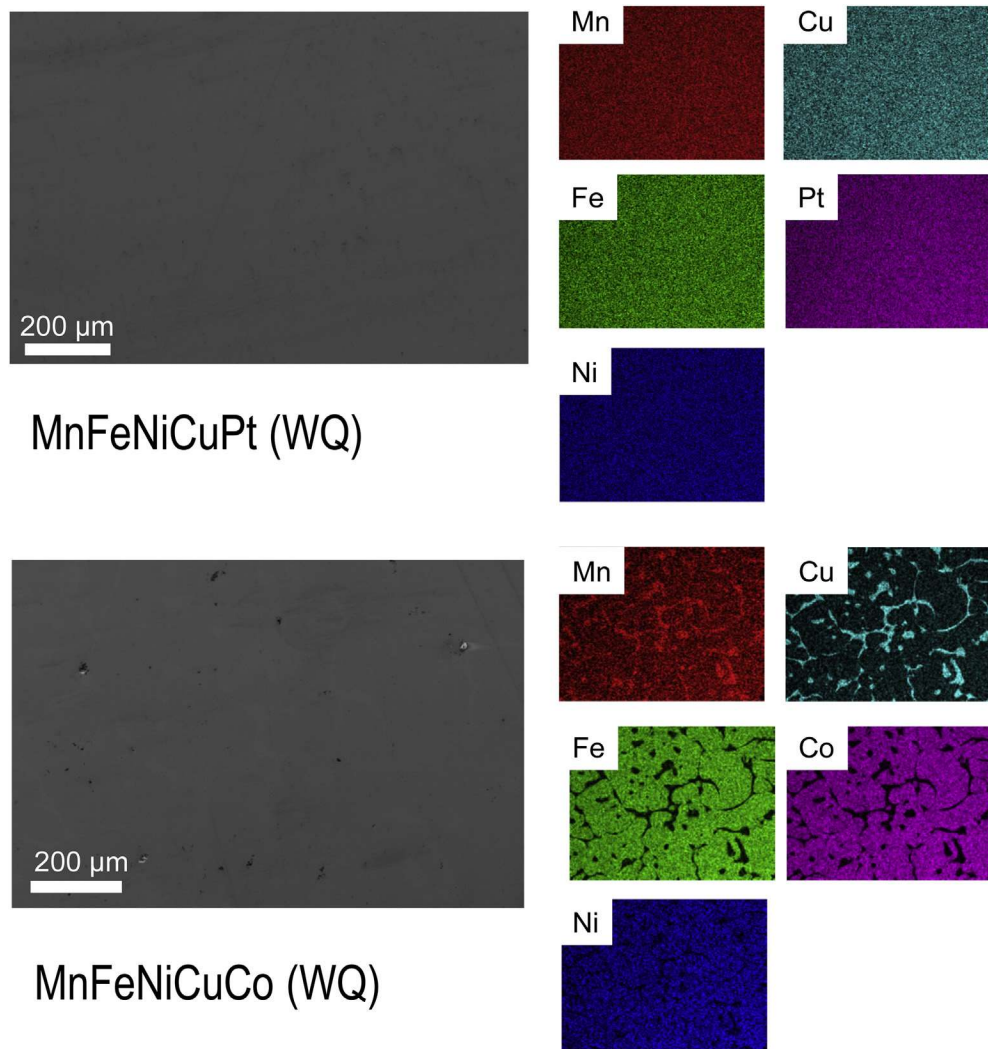


Fig. 4. SEM images and EDX maps of the MnFeNiCuPt and MnFeNiCuCo alloys annealed at 1373 K for 43.2 ks with subsequent WQ.

Table 1

Values of $\Delta H_{\text{mix}}/\text{kJ mol}^{-1}$ acquired from Miedema's scheme listed on the upper-right side and those from SSOL4 database calculated with conditions of $\Omega/4 = (\Delta H_{\text{mix}})$ at 900 K on the lower-left side, all for binary liquid phase at equi-atomic composition. Ω of the Pt-containing alloys cannot be provided by SSOL4.

SSOL4↓	Miedema→					
	Mn	Fe	Ni	Cu	Pt	Co
Mn		0	-8	4	-28	-5
Fe	-0.9		-2	13	-13	-1
Ni	-14.9	-3.1		4	-5	0
Cu	-2.3	8.5	3.3		-12	6
Pt	-	-	-	-		-7
Co	-7.4	-2.3	0.3	8.2	-	

immiscible tendency between (Fe,Co) and (Cu,Mn). Empirically, these tendencies were evaluated in terms of mixing enthalpy (ΔH_{mix}) [20,21] by sign, where the negative and positive values of ΔH_{mix} respectively enhance the formation of amorphous (or ordered crystalline) phases and immiscible phases. The values of ΔH_{mix} summarized in Table 1 were acquired from literature based on Miedema's empirical method [20,21] and from SSOL4 database as calculated at 900 K in the present study. The negative sign of ΔH_{mix} in Table 1 partially explains the preferential tendency to form

solid solutions in Fe and Pt as (Fe,Pt) as well as (Fe,Co) as shown in Fig. 3. Among the values of ΔH_{mix} in Table 1, the largest values are given for Fe-Cu as $\Delta H_{\text{mix}} = 13$ and 8.5 kJ mol^{-1} for Miedema's model and the SSOL4 database, respectively. These ΔH_{mix} values for Fe-Cu support the immiscible tendency between Fe and Cu, resulting in the preferences of (Fe,Pt) and (Cu,Mn) for the MnFeNiCuPt alloy and (Fe,Co) and (Cu,Mn) for the MnFeNiCuCo alloy. On the other hand, the large, negative value given in Table 1 for Mn-Pt as $\Delta H_{\text{mix}} = -28 \text{ kJ mol}^{-1}$ by Miedema's model disagrees with the formation of solid solutions of (Fe,Pt) and (Cu,Mn) as shown in Fig. 3. Instead, it explains the formation of an L1₂ ordered phase in the MnFeNiCuPt alloy subjected to FC, as shown in Fig. 2(b). In addition, the formation of solid solutions of (Fe,Pt) and (Cu,Mn) cannot be explained by an immiscible tendency between Mn and Cu with $\Delta H_{\text{mix}} = 4 \text{ kJ mol}^{-1}$ by Miedema's model, although the SSOL4 database gives $\Delta H_{\text{mix}} = -2.3 \text{ kJ mol}^{-1}$. While the details of the atomic preferences cannot be comprehensively explained, it is possible that the immiscible tendency between Fe and Cu determines the experimentally observed phase separation (Fig. 3).

Table 1 shows that the Cu₅₀Mn₅₀ (at.%) alloy with a liquid structure gives $\Delta H_{\text{mix}} = 4 \text{ kJ mol}^{-1}$ from Miedema's model and $\Delta H_{\text{mix}} = -2.3 \text{ kJ mol}^{-1}$ from the SSOL4 database. The former case of ΔH_{mix} by Miedema's model does not support the experimentally

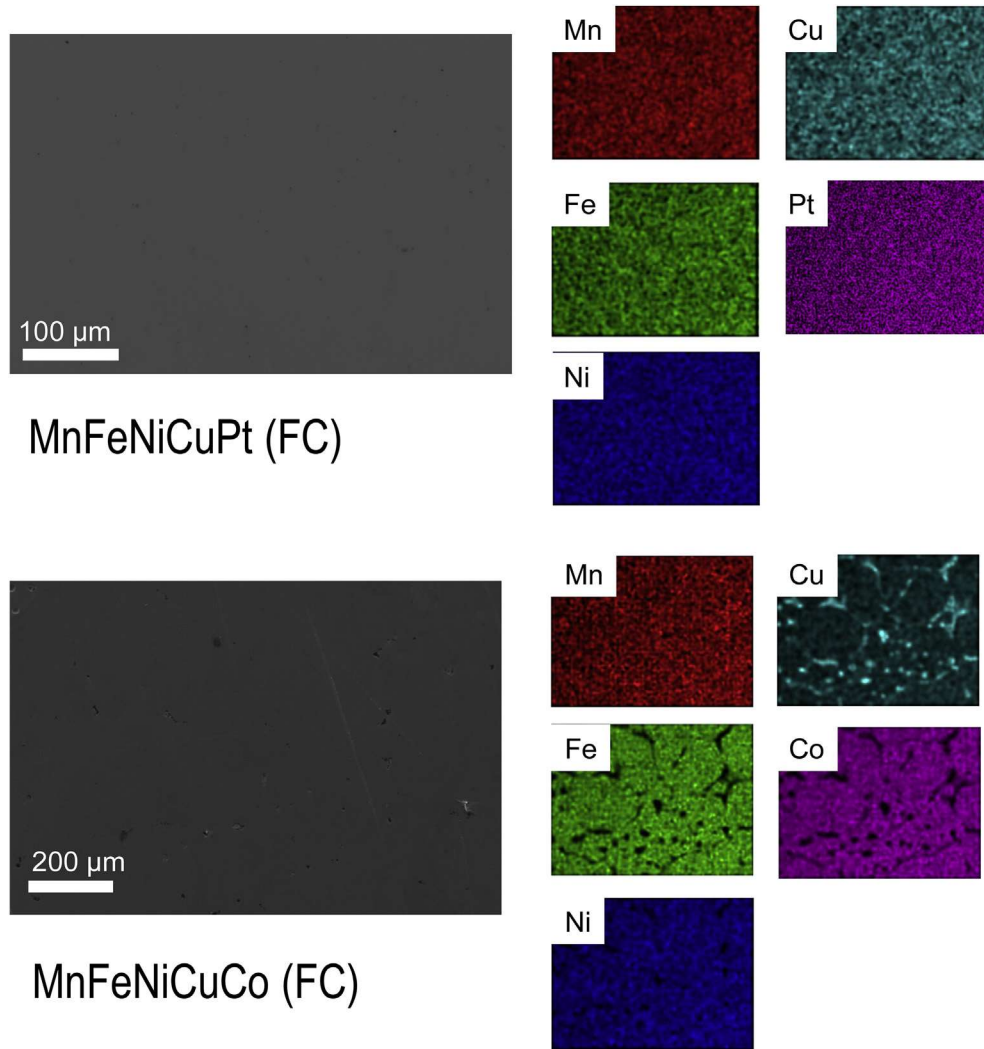


Fig. 5. SEM images and EDX maps of the MnFeNiCuPt and MnFeNiCuCo alloys annealed at 1373 K for 43.2 ks with subsequent FC.

observed attractive tendency between Cu and Mn (Fig. 3). In part, this disagreement of ΔH_{mix} between Mn and Cu is due to the fact that Cu is not regarded as a transition metal in Miedema's model [20]. Thus, further analysis was performed based on a thermodynamic approach with Thermo-Calc by using the SSOL4 database for solid solutions based on the CALPHAD model, which enables us to download the interaction parameter (\mathcal{Q}) as a function of composition and temperature. The compositional dependence of \mathcal{Q} can be ignored for exact equi-atomic alloys with A₅₀B₅₀ (at.%) in a binary system, since \mathcal{Q} is provided in an algebraic representation [22] with n-th order terms as $\mathcal{Q}^{(n)}(c_A - c_B)^n$, where c_A and c_B are contents of elements A and B, respectively, and $\mathcal{Q}^{(n)}$ is the n-th order coefficient of \mathcal{Q} . Specifically, $c_A = c_B = 0.5$ for the A₅₀B₅₀ alloy, resulting in $\mathcal{Q} = \mathcal{Q}^{(0)}$ as a function of temperature, which is usually given as an algebraic representation up to the first order. In the SSOL4 database, $\mathcal{Q}^{(0)}$ of the Cu-Mn liquid can be derived as $\mathcal{Q}^{(0)}/4 (= \Delta H_{\text{mix}}) = 1.800 - 2.28 \times 10^{-3} T/\text{kJ mol}^{-1}$ at a temperature range of $T = 298.15 - 3000$ K, suggesting that $\mathcal{Q}/4 (= \Delta H_{\text{mix}}) < 0 \text{ kJ mol}^{-1}$ for $T > 798$ K. This modified value of $\Delta H_{\text{mix}} < 0 \text{ kJ mol}^{-1}$ based on the CALPHAD method explains the behavior of Cu-Mn as shown in Fig. 3. This suggests that the solid solutions of (Cu,Mn) were formed in the MnFeNiCuPt and MnFeNiCuCo alloys during cooling at temperatures of $T > 798$ K, enabling effective atomic diffusions to occur.

The formations of a single fcc and dual fcc phases in the annealed MnFeNiCuPt and MnFeNiCuCo alloys can be discussed in terms of atomic size differences. The behaviors of the as-prepared MnFeNiCuPt and MnFeNiCuCo alloys is akin to single fcc phase based on XRD, as shown in Fig. 1(a,d). Table 2 summarizes r_i for fcc or as a Gold-Schmidt value acquired from the literature [23,24]. The r_i 's of the constituent elements are almost the same among Mn, Fe, Co, Ni and Cu with r_i ranging 0.123–0.128 nm, whereas Pt has $r_{\text{Pt}} = 0.139$ nm. Judging from r_i , it is possible that the as-prepared MnFeNiCuCo alloy exhibits a single phase in XRD regardless of the actual dual phases on the microscopic scale as shown in Fig. 3. The annealed MnFeNiCuPt alloy can behave as a single phase as long as the dual phases are solid solutions, since r_i values of the constituent elements occupy a narrow range. More specifically, the average atomic radius (\bar{r}) of the fcc structure of these alloys can be evaluated from Fig. 2 for using their lattice constants, a , as $\bar{r} = \sqrt{2}a/4$, or $\bar{r} = 0.132$ and 0.128 nm respectively for the as-prepared MnFeNiCuPt and MnFeNiCuCo alloys. For the MnFeNiCuCo alloy, $\bar{r} = 0.128$ nm which is very close to r_{Cu} , implying that the dual phases would not cause large lattice distortions due to their small differences in r_i . On the other hand, $\bar{r} = 0.132$ nm for the MnFeNiCuPt alloys is just the average value between $r_{\text{Pt}} = 0.139$ nm and $r = 0.125$ nm, the latter of which is an average of the other constituent elements (Mn, Fe, Co, Ni and Cu; 0.124–0.128 nm).

Table 2

Atomic radii (r_i) for fcc or as a Gold-Schmidt value acquired from literature [22,23].

Mn	Fe	Co	Ni	Cu	Pt	
r_i/nm	0.123* [23]	0.124 [22]	0.125 [22]	0.125 [22]	0.128 [22]	0.139 [22]

*Estimated from literature $a_{\text{fcc}} = 0.349 \text{ nm}$ [23].

These r_i characteristics explain the formation of the single phase in the annealed MnFeNiCuPt alloy.

Further investigations of the MnFeNiCuPt and MnFeNiCuCo alloys were carried out computationally to study their equilibrium phases as a function of temperature, using a similar thermodynamic analysis based on Thermo-Calc with SSOL5 database as well as TCHEA1 as a reference. Fig. 6(a) demonstrates that the MnFeNiCuPt alloy computed with the SSOL5 database exhibits a single fcc phase at temperatures ranging from 1544 to 1130 K, followed by the dual fcc phases down to 340 K with subsequent multi-phases comprised of fcc and small amounts of bcc phases, although the phase separation at $T < 340 \text{ K}$ would not take place kinetically. On the other hand, Fig. 6(b) shows that the MnFeNiCuCo alloy examined with the SSOL5 database gives a fcc phase precipitate from a melt at $T \approx 1552 \text{ K}$, followed by the secondary precipitation of another fcc phase to form dual fcc phases at temperatures as low as 764 K. A bcc phase and another fcc phase then precipitate in sequence as temperature decreases. When the temperature reaches $T \approx 482 \text{ K}$, a eutectoid reaction takes place to form a mixed structure of fcc, L1₀ and B2 phases. The MnFeNiCuCo alloy examined with the TCHEA1 database (Fig. 6(c)) exhibits a single fcc phase at temperatures ranging 1430 to 1004 K, followed by dual fcc phases while decreasing temperature to 831 K. The mixture of dual fcc and B2 phases remained at 690 K, which can be regarded as a eutectoid temperature. Further decreasing temperature caused an increased amount of L1₀ phase to be present. Comparisons with Fig. 6(b) and (c) revealed that the details of the species present in these phases and their amounts changed with temperature, confirming that a single or dual fcc phase is stable at temperatures between the solidus line (~1500 K) and the eutectoid temperature

(~700 K) or lower. The eutectoid temperature in Fig. 6(c) is higher than that in Fig. 6(b), suggesting that the MnFeNiCuPt may have a higher eutectoid temperature if computed with the TCHEA1 database in future versions. Fig. 6 indicates that the MnFeNiCuPt and MnFeNiCuCo alloys exhibit dual fcc phases around 800–1100 K, supporting the experimental data (Fig. 3) of dual fcc phase transformation during cooling. Liquidus and solidus temperatures (T_l and T_s) respectively were calculated as 1664.3 and 1544.5 K for the MnFeNiCuPt alloy (Fig. 6(a)), 1551.7 and 1324.1 K for the MnFeNiCuCo alloy (Fig. 6(b)), and 1541.7 and 1430.3 K for the MnFeNiCuCo alloy (Fig. 6(c))). The theoretical analysis in Fig. 6 revealed that calculations based on the SSOL5 database agree with the experimental data, in that the MnFeNiCuPt and MnFeNiCuCo alloys can be formed into single and dual fcc phases respectively at temperatures of approximately 1373 K.

The components of the phases as computed at $T = 900 \text{ K}$ are summarized in Table 3, indicating that dual fcc phases are principally rich in (Mn, Fe, Ni) for all calculations, denoted by FCC_#1. The other phases are rich in Cu and Pt for the MnFeNiCuPt alloy and Cu and Co for the MnFeNiCuCo alloy for the SSOL5 database, and Cu-rich for the TCHEA1 database. The homogeneous distribution of Ni experimentally shown in Fig. 3 was not reproduced in the calculations, but the calculation results demonstrate the tendency of phase separation between the fcc structures. The results shown in Fig. 6 and Table 3 suggest that the MnFeNiCuPt and MnFeNiCuCo HEAs with dual fcc phases observed in the as-prepared samples in Fig. 3 were prepared during cooling from a melt by passing through a single fcc phase at $T \approx 1200 \text{ K}$, followed by a second phase appearance at $T \approx 900 \text{ K}$. The L1₂ ordered phase that appeared in the annealed MnFeNiCuPt alloy subjected to FC was not reproduced

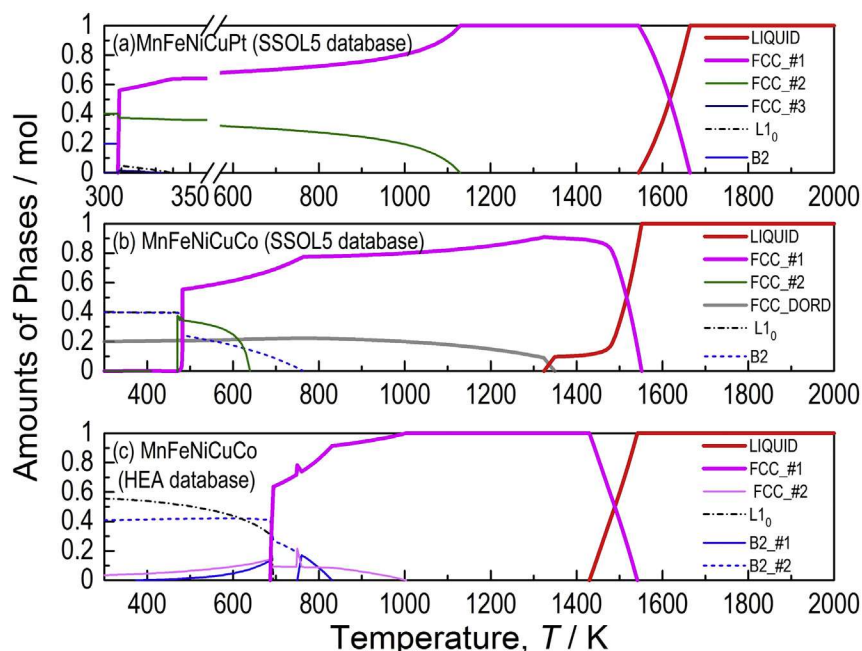


Fig. 6. Thermodynamic assessments of the MnFeNiCuPt and MnFeNiCuCo alloys using Thermo-Calc with databases of SSOL5 for (a) MnFeNiCuPt and (b) MnFeNiCuCo alloys and of (c) TCHEA1 for the MnFeNiCuCo alloy.

Table 3

Equilibrium phases, compositions of contents and amounts of moles in 1 mol of alloy for the MnFeNiCuPt and MnFeNiCuCo alloys calculated at 900 K with the SSOL5 database for solid solutions and the MnFeNiCuCo alloy calculated at 900 K with the TCHEA1 database. The bold letters indicate the major components of each phase.

	Database	Mn	Fe	Ni	Cu	Pt	Co	Amounts of moles
FCC_#1	SSOL5	24.063	26.031	25.082	7.564	17.260	—	0.755
FCC_#2		7.479	1.415	4.340	58.323	28.443	—	0.245
FCC_#1	SSOL5	25.453	25.453	25.453	2.612	—	21.029	0.786
FCC_DORD		0	0	0	83.775	—	16.225	0.214
FCC_#1	TCHEA1	20.821	21.241	20.897	15.816	—	21.225	0.941
FCC_#2		6.933	0.258	5.741	86.545	—	0.523	0.059

from thermodynamic analysis. Presumably, this is due to the shortness of the SSOL5 database. However, the presence of a single phase at 1373 K was correctly explained as shown in Fig. 6(a). Finally, the magnetic properties of the as-prepared MnFeNiCuPt and MnFeNiCuCo alloys were investigated with VSM as shown in Fig. 7. The hysteresis curves measured by VSM indicate that the as-prepared MnFeNiCuPt and MnFeNiCuCo alloys exhibit soft magnetism with a coercivity of approximately 1.2 kA m⁻¹ where the saturation magnetization (M_s) was approximately 0.23 T and 0.43 T, respectively. The higher M_s for the MnFeNiCuCo than MnFeNiCuPt can be explained by the inclusion of Co as a ferromagnetic element as well as Fe and Ni in the MnFeNiCuCo alloy. Simultaneous inclusions of ferromagnetic elements (Fe, Ni and Co) do not enhance M_s due to the equi-atomic strategy for deciding the constituent elements. This is a disadvantageous aspect of HEAs when ferromagnetic alloys are desired, and merits investigation for future research. The magnetic measurements of the annealed MnFeNiCuPt and MnFeNiCuCo alloys subjected to WQ and FC revealed that they exhibited soft magnetism, as shown in Fig. 7 for the AP samples. However, the results of the WQ and FC samples are not shown in Fig. 7 because of the cavities in the WQ and FC samples, which degrade the measurement accuracy.

4. Conclusions

XRD analysis and SEM observation together with EDX analysis revealed that quinary exact equi-atomic MnFeNiCuPt and MnFeNiCuCo alloys as-prepared by induction melting method formed into high-entropy alloys (HEAs) with dual fcc structures comprising

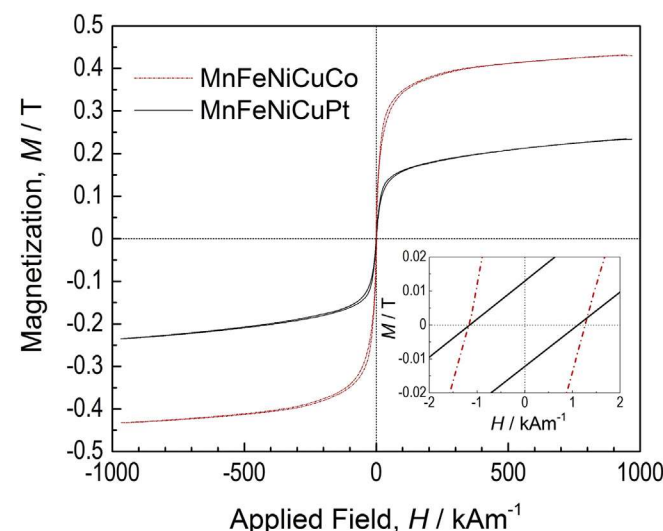


Fig. 7. VSM measurements of the AP MnFeNiCuPt and MnFeNiCuCo alloys where the samples were measured with the long axis of the rectangular samples parallel to the direction of solidification (bottom to top of button samples).

dendrites on the 10 μm scale. The dual fcc phases behave as a single phase from XRD and DTA analysis, presumably because of the small difference in lattice constants between the dual phases. In order to clarify the equilibrium phases, the samples were annealed at 1773 K for 43.2 ks, followed by water quenching (WQ) and furnace cooling (FC). The annealed MnFeNiCuPt and MnFeNiCuCo alloys subjected to WQ respectively formed into a single fcc phase and dual fcc phases. On the other hand, the MnFeNiCuPt and MnFeNiCuCo alloys subjected to FC respectively formed into a single L1₂ ordered phase and dual fcc phases. These formations of single and dual phases at 1373 K as indicated by EDX analysis were explained by thermodynamic calculations with Thermo-Calc using the SSOL5 database for solid solutions. Measurement of magnetic properties for saturation magnetization (M_s) and coercivity (H_c) revealed that both MnFeNiCuPt and MnFeNiCuCo alloys featured soft magnetism where $M_s \approx 0.23$ T for the MnFeNiCuPt alloy and $M_s \approx 0.43$ T for the MnFeNiCuCo alloy, both alloys had $H_c \approx 1.2$ kA m⁻¹. This alloy design motif, focusing on an L1₀ structure from Pettifor map for binary compounds with 1:1 stoichiometry, is a new pathway for discovering new HEAs.

Acknowledgements

The research was supported in part by a Grant-in-Aid for Scientific Research from the Japan Society for the Promotion of Science (JSPS): Grant Program of Scientific Research (B) with program title of “Fabrication of High-Entropy Bulk Metallic Glasses based on Confusion Principle, Clarification of their Properties and their Application” (grant number 24360284).

References

- [1] J.W. Yeh, S.K. Chen, S.J. Lin, J.Y. Gan, T.S. Chin, T.T. Shun, C.H. Tsau, S.Y. Chang, Nanostructured high-entropy alloys with multiple principal elements: novel alloy design concepts and outcomes, *Adv. Eng. Mater.* 6 (2004) 299–303.
- [2] J.W. Yeh, Recent progress in high-entropy alloys, *Ann. De. Chim. Sci. Des. Mater.* 31 (2006) 633–648.
- [3] Thermodynamic and Mobility Databases Overview, 2016. http://thermocalc.videmar.se/media/32320/db-overview_20151130.pdf (Accessed 17 March 2016).
- [4] “Thermo-calc Software”, <http://www.thermocalc.com/start/>, (Accessed 16 December 2015).
- [5] Y.J. Zhou, Y. Zhang, Y.L. Wang, G.L. Chen, Solid solution alloys of AlCoCrFeNiTiX with excellent room-temperature mechanical properties, *Appl. Phys. Lett.* 90 (2007).
- [6] O.N. Senkov, J.M. Scott, S.V. Senkova, D.B. Miracle, C.F. Woodward, Microstructure and room temperature properties of a high-entropy TaNbHfZrTi alloy, *J. Alloy Compd.* 509 (2011) 6043–6048.
- [7] B. Cantor, I.T.H. Chang, P. Knight, A.J.B. Vincent, Microstructural development in equiatomic multicomponent alloys, *Mater. Sci. Eng. A Struct.* 375 (2004) 213–218.
- [8] F. Otto, Y. Yang, H. Bei, E.P. George, Relative effects of enthalpy and entropy on the phase stability of equiatomic high-entropy alloys, *Acta Mater.* 61 (2013) 2628–2638.
- [9] A. Takeuchi, K. Amiya, T. Wada, K. Yubuta, W. Zhang, High-entropy alloys with a hexagonal close-packed structure designed by equi-atomic alloy strategy and binary phase diagrams, *Jom Us* 66 (2014) 1984–1992.
- [10] M. Feuerbacher, M. Heidelmann, C. Thomas, Hexagonal high-entropy alloys, *Mater. Res. Lett.* 3 (2015) 1–6.
- [11] C.J. Tong, Y.L. Chen, S.K. Chen, J.W. Yeh, T.T. Shun, C.H. Tsau, S.J. Lin, S.Y. Chang,

- Microstructure characterization of $\text{Al}_x\text{CoCrCuFeNi}$ high-entropy alloy system with multiprincipal elements, *Metall. Mater. Trans. A* 36A (2005) 881–893.
- [12] A.K. Singh, A. Subramaniam, On the formation of disordered solid solutions in multi-component alloys, *J. Alloy Compd.* 587 (2014) 113–119.
- [13] A. Takeuchi, K. Amiya, T. Wada, K. Yubuta, Alloy design for high-entropy alloys based on Pettifor map for binary compounds with 1:1 stoichiometry, *Intermetallics* 66 (2015) 56–66.
- [14] Tazuddin, K. Biswas, N.P. Gurao, Deciphering micro-mechanisms of plastic deformation in a novel single phase fcc-based MnFeCoNiCu high entropy alloy using crystallographic texture, *Mater. Sci. Eng. A* 657 (2016) 224–233.
- [15] Y. Zhang, Y.J. Zhou, J.P. Lin, G.L. Chen, P.K. Liaw, Solid-solution phase formation rules for multi-component alloys, *Adv. Eng. Mater.* 10 (2008) 534–538.
- [16] A. Manzoni, H. Daoud, R. Volkl, U. Glatzel, N. Wanderka, Phase separation in equiatomic AlCoCrFeNi high-entropy alloy, *Ultramicroscopy* 132 (2013) 212–215.
- [17] X.D. Xu, P. Liu, S. Guo, A. Hirata, T. Fujita, T.G. Nieh, C.T. Liu, M.W. Chen, Nanoscale phase separation in a fcc-based $\text{CoCrCuFeNiAl}_{0.5}$ high-entropy alloy, *Acta Mater.* 84 (2015) 145–152.
- [18] Y.F. Ye, Q. Wang, Y.L. Zhao, Q.F. He, J. Lu, Y. Yang, Elemental segregation in solid-solution high-entropy alloys: experiments and modeling, *J. Alloy Compd.* 681 (2016) 167–174.
- [19] S. Sohn, Y. Liu, J. Liu, P. Gong, S. Prades-Rodel, A. Blatter, B.E. Scanley, C.C. Broadbridge, J. Schroers, Noble metal high entropy alloys, *Scr. Mater.* 126 (2017) 29–32.
- [20] F.R. de Boer, R. Boom, W.C.M. Mattens, A.R. Miedema, A.K. Nissen, Cohesion in Metals: Transition Metal Alloys, North Holland Physics Publishing, a Division of Elsevier Scinece Publishers B.V, The Netherlands, 1988.
- [21] A. Takeuchi, A. Inoue, Classification of bulk metallic glasses by atomic size difference, heat of mixing and period of constituent elements and its application to characterization of the main alloying element, *Mater. Trans.* 46 (2005) 2817–2829.
- [22] O. Redlich, A.T. Kister, Algebraic representation of thermodynamic properties and the classification of solutions, *Ind. Eng. Chem.* 40 (1948) 345–348.
- [23] Metal Databook, fourth ed., Maruzen Co. Ltd., Tokyo, 2004.
- [24] Pearson's Crystal Data: Crystal Structure Database for Inorganic Compounds (on CD-ROM), ASM International, Materials Park, OH, U.S.A, 2011.